Meccanica (2016) 51:371–381
DOI 10.1007/s11012-015-0280-3

Strain-gradient crystal-plasticity modelling of micro-cutting of b.c.c. single crystal

Murat Demiral · Anish Roy · Vadim V. Silberschmidt

Received: 7 January 2015 / Accepted: 4 September 2015 / Published online: 5 October 2015

Abstract In recent years thanks to enhancements in design of advanced machines, laser metrology and computer control, ultra-precision machining has become increasingly important. In micromachining of metals the depth of cut is usually less than the average grain size of a polycrystalline aggregate; hence, a cutting process can occur entirely within a single crystal. The respective effect of crystallographic anisotropy requires development of machining models that incorporate crystal plasticity for an accurate prediction of micro-scale material removal under such conditions. To achieve this, a 3D finite-element model of orthogonal micro-cutting of a single crystal of b.c.c. brass was implemented in a commercial software ABAQUS/Explicit using a user-defined subroutine VUMAT. Strain-gradient crystal-plasticity theories were used to demonstrate the influence of evolved strain gradients on the cutting process for different cutting directions.

M. Demiral
Department of Mechanical Engineering, University of Turkish Aeronautical Association, 06790 Ankara, Turkey

A. Roy (✉) · V. V. Silberschmidt
Wolfson School of Mechanical and Manufacturing Engineering, Loughborough University, Loughborough LE11 3TU, UK
e-mail: A.Roy3@lboro.ac.uk

Keywords Strain-gradient crystal-plasticity · Orthogonal micro-cutting · Brass single crystal · Finite-element analysis

1 Introduction and motivation

With continuous miniaturization of industrial products, understanding of micro-scale deformation of materials increases in its significance. In micromachining of metals, the depth of cut is usually less than the average grain size of a polycrystalline aggregate. As a result, the cutting action may occur entirely within a single crystal. In the experimental micromachining studies, such parameters as the cutting force, shear angle, dynamic shear stress and chip thickness were observed to depend on the orientation of the cutting direction and the cutting-plane normal with respect to the crystal axis. This is naturally explained by the fact that single crystals are highly anisotropic in their physical properties [1]. To elucidate the underlying physics for the micro-machining process, different analytical and numerical models were proposed.

Sato [2] tried to use the continuum yield theory to analyse changes in the shear stress and shear angle with material anisotropy, but the attempt was unsuccessful as the value of the shear angle was in the reverse phase to shear stress. Later, Sato et al. [3] calculated the shear angle from the vector sum of slip directions on active slip systems based on the assumption that the amount of shearing on the slips

system is proportional to its Schmid factor. Shirakashi et al. [4] used the Hill's orthogonal plastic anisotropy theory to predict shear angles in cutting f.c.c. single crystals. This approach, however, was found to be not suitable for predicting machining forces. Lee and Zhou [5] and Lee et al. [6] used an effective Taylor factor to predict a shear angle in single-crystal cutting. For each crystallographic orientation, this factor was calculated for all possible shear angles. However, it was observed (based on the minimum energy criterion) that a range of shear angles might exist for a given type of material's anisotropy. The authors proposed that the most likely shear angle was the one corresponding to the most negative texture-softening factor among the ones with the same minimum shear strength. This work was then extended using the Merchant's model to predict the change in cutting forces with crystallographic orientation. Recently, Kota and Ozdoganlar [7] developed a plasticity-based model of a machining force combining the Bishop and Hill's crystal plasticity models with the Merchant's orthogonal cutting model; the experimental validation of the model was carried out. All these analytical models were developed based on assumption of plain-strain orthogonal cutting.

Continuum numerical models of micro-scale material removal processes compared to analytical ones are limited. Liang et al. [8] attempted to predict the effects of crystal orientation and grain boundaries on cutting forces using 2D finite-element (FE) analysis. However, in the study deformation was confined only to the elastic region. Liu and Melkote [9] developed a 3D FE model of micro-cutting including strain-gradient effects. In their study the crystallographic anisotropy was not accounted for in the constitutive equations. Recently, Zahedi et al. [10] and Demiral et al. [11] investigated the effect of crystallographic anisotropy on a response of copper single crystal using a 3D smoothed particle hydrodynamics/FE crystal plasticity model and a strain-gradient crystal-plasticity FE model, respectively. This technique has been shown to have much promise.

Recent experiments have demonstrated that metallic materials display a strong size effect at the micron and sub-micron scales [12, 13]. This phenomenon was attributed to the presence of geometrically necessary dislocations (GNDs) associated with nonuniform plastic deformation. In this regard, it becomes essential to account for strain gradients, arising in cutting processes, for accurate prediction of micro-scale material removal in machining models. Since conventional crystal-plasticity theories possess no intrinsic material lengths, these cannot explain the size-dependent material's behaviour at small scales. In this study, an enhanced modelling scheme of a lower-order strain-gradient crystal-plasticity (EMSGCP) theory proposed by Demiral [14] is used. This work aims to demonstrate the influence of lower-order strain gradients on the deformation response of b.c.c. single-crystal brass in the machining process. In contrast to lower-order gradient theories, higher-order theories incorporate an additional partial differential equation accounting for strain gradient effects, requiring extra boundary conditions, which are often difficult to determine [15–18].

This paper is organized as follows: the details of the developed finite-element model of micro-cutting are introduced in Sect. 2. Section 3 presents its validation against experimental data and demonstrates its predictive capabilities for different cutting directions. Finally, we conclude with some remarks in Sect. 4. The theory for a strain-gradient crystal-plasticity model with governing equations is presented in "Appendix".

2 Finite-element implementation

A FE model of the orthogonal micro-machining experiment on a workpiece with dimensions 20 μm × 20 μm × 0.48 μm (Fig. 1) was developed [11]. Considering a compromise between the accuracy and computation time, 29,600 eight-node linear brick elements (C3D8) were used to discretise the sample, with a minimum element size of 60 nm in the process zone. The cutting tool, modelled as a rigid body with rake and clearance angles of 0°, was displaced in the cutting direction ([abc] in Fig. 1) with a velocity of −1300 mm/s. A depth of cut (a_p) was fixed at 0.8 μm and the maximum cutting length of 1.75 μm was considered in the simulations. Friction was neglected throughout the simulation. Chip separation from the workpiece material was achieved with the use of an element-deletion module available in ABAQUS/Explicit [19]; the Taylor cumulative shear strain on all slip systems ($\tilde{\gamma}$) was employed as the failure criteria. Shear failure is assumed to occur when this parameter reached a critical value of 3.

Here, machining in a single crystal of β-brass with a b.c.c. crystalline structure is studied. It was known that

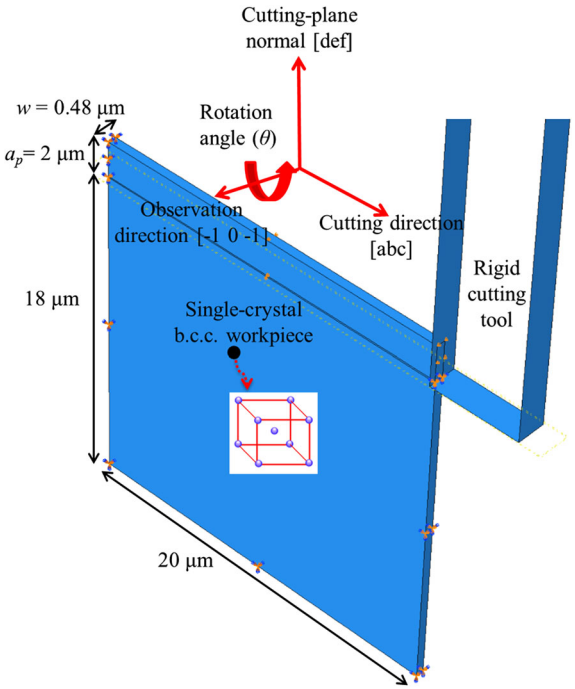

Fig. 1 Dimensions and coordinate system for orthogonal cutting of single-crystal workpiece material

the active slip system of this structure is {110}<111> [16]; therefore, only this set—from three potential system in b.c.c. materials—was enabled in the simulations. Three material parameters, $C_{11} = 131.0$ GPa, $C_{12} = 115.0$ GPa, $C_{44} = 92.0$ GPa, were used to define the elasticity tensor for the β-brass crystal [17], with its density 8500 kg/m^3; the respective plasticity parameters used in the simulations are listed in Table 1. Standard damping parameters of 0.06 and 1.2 for linear and quadratic bulk viscosity, respectively, were used. A mass scaling factor was set at 1000 to improve computational speed. This led to an increase in time increment by a factor of ~ 33 to $\Delta t = 3.15 \times 10^{-10}$ s, without compromising numerical accuracy.

Table 1 Plastic parameters used in FE simulations [11, 21–25]

$\dot{\gamma}_0^\alpha$ (s^{-1})	10^{-3}	K (MPa mm)	0.04
n	20	μ (GPa)	27.12
q	1	b (mm)	2.56×10^{-7}
h_0 (MPa)	294	$\rho_s\|_{t=0}$ (mm^{-2})	6.8×10^5
$g_T^\alpha\|_{sat}$ (MPa)	60	$\rho\|_{t=0}$ (mm^{-2})	5.0×10^4
α_T	0.8	$\bar{S}/\bar{V}$	4.36

The simulations were performed using the EMSGCP and enhanced modelling scheme of crystal-plasticity (EMCP) theories implemented in the finite-element code ABAQUS/Explicit [15] using the user-defined material subroutine (VUMAT). Their comparison elucidates the amount of evolving strain gradients during the deformation process. A summary of the theories is given in "Appendix".

3 Results and discussion

In this section, results of the FE simulations of orthogonal micro-cutting of single-crystal β-brass are presented. To assess the effect of rotation angle θ for a crystal with the [101] axis parallel to the observation direction (Fig. 1) on the shear angle ϕ, seven cutting directions, viz. $\theta = -45°$, $-35°$, $-20°$, 0°, 20°, 35° and 45°, were chosen. The corresponding values are listed in Table 2.

Figure 2 demonstrates chip shapes obtained in FE simulations based on the EMSGCP theory for different rotation angles of the (1 0 1) β-brass. Apparently, ϕ varies remarkably with θ, resulting in the corresponding values of 52°, 54°, 37°, 44°, 46°, 53° and 44° for $\theta = -45°$, $-35°$, $-20°$, 0°, 20°, 35° and 45°, respectively (Fig. 3).

In ultra-precision machining, a large shear angle is associated with continuous chip formation and good surface finish [26]. Therefore, among the cutting directions investigated here, $\theta = -45°$, $-35°$ and 35° are preferable for micro-cutting of brass single crystals for a better surface finish. To check the accuracy of the model, the obtained results were compared with the experiments presented in [20]. Our FE results demonstrated that the shear angles were predicted reasonably

Table 2 Different cutting directions ([abc]) and cutting-plane normals ([def]) for different θ values of [1 0 1] axis parallel to the observation direction (see Fig. 1)

θ	[abc]	[def]
−45°	[1.414 −2 −1.414]	[−1 −1.414 1]
−35°	[0.990 −2 −0.990]	[−1 −0.990 1]
−20°	[0.515 −2 −0.515]	[−1 −0.515 1]
0°	[0 −1 0]	[−1 0 1]
20°	[−0.515 −2 0.515]	[−1 0.515 1]
35°	[−0.990 −2 0.990]	[−1 0.990 1]
45°	[−1.414 −2 1.414]	[−1 1.414 1]

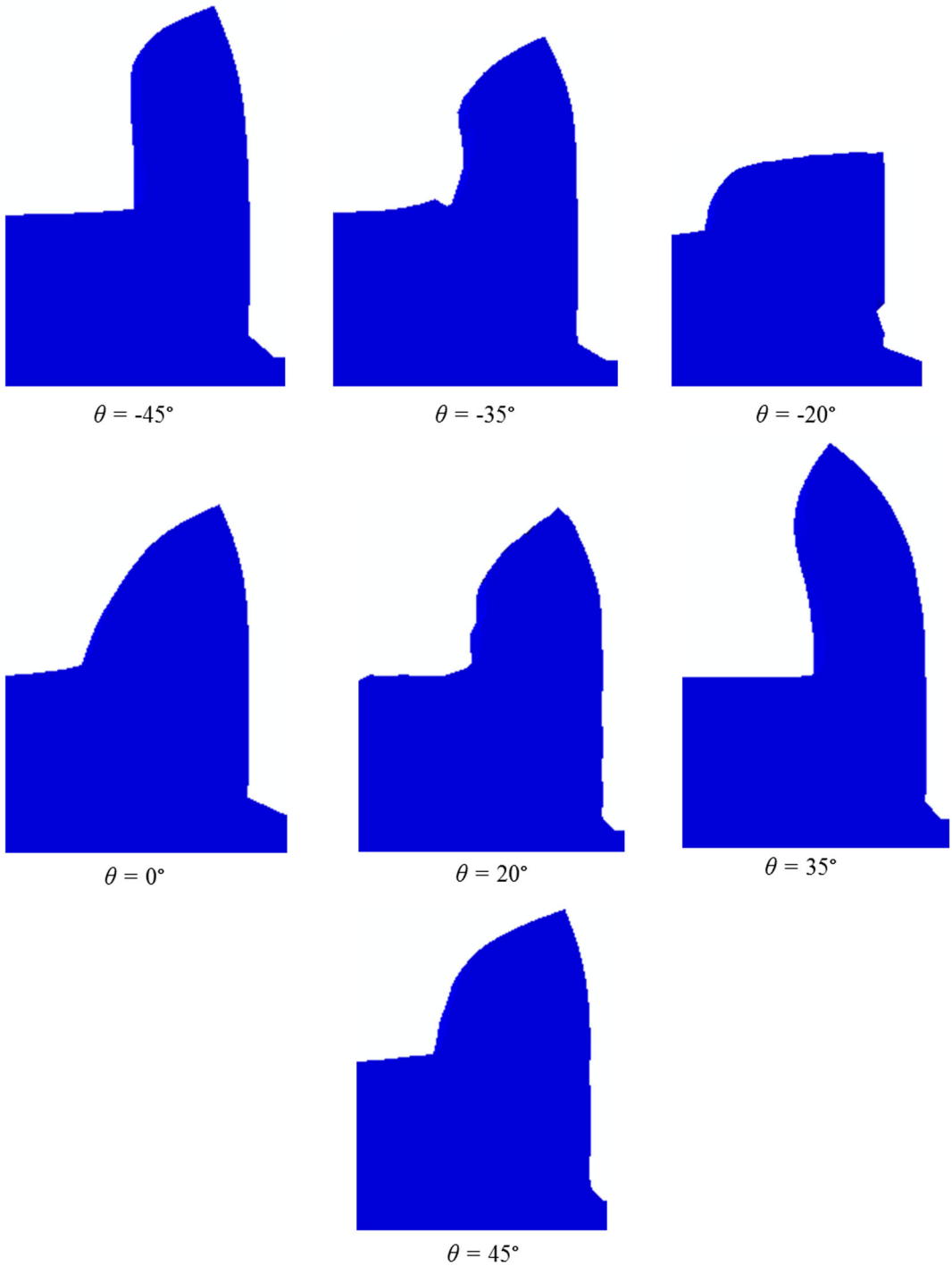

Fig. 2 Numerically obtained chip morphologies at cutting length of 1.0 μm for different rotation angles of (1 0 1) β-brass

close except for $\theta = -20°$ and $\theta = 0°$. However, the general trends of the curves describing a variation of ϕ for different θ values, obtained numerically and experimentally, were in good agreement.

Figure 3 presents also the analytical results based on the analysis of the Schmid factor reported in [20]. Although the shear angles were captured successfully for $\theta = -20°$ and $\theta = 0°$ with this approach, a

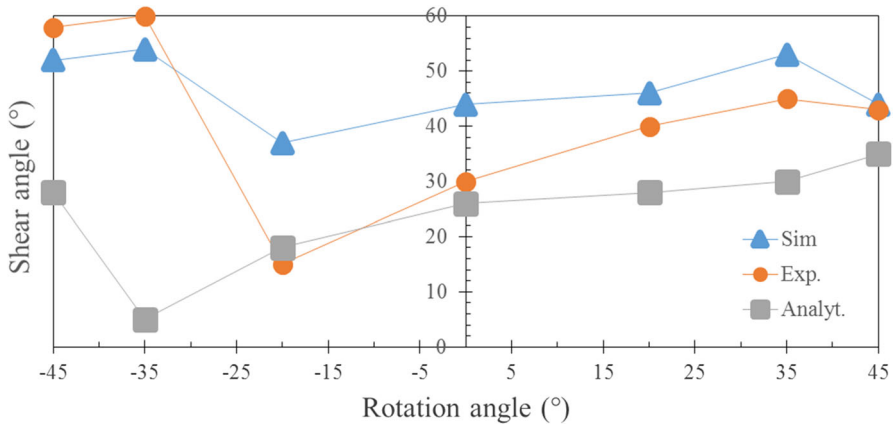

Fig. 3 Variation of shear angle with rotation angle obtained in experiments [20], simulations (via the EMSGCP theory) and analytical solutions [20] for (1 0 1) β-brass

significant deviation was observed for other values, especially for $\theta = -45°$ and $\theta = -35°$. These results suggest that our numerical predictions are more in accord with the experiments when compared to the analytical ones. It should be emphasized that the frictional, thermal and viscous effects were not accounted in the present model; this might be one of the reasons for overestimation of ϕ values at $\theta = -20°$ and $\theta = 0°$ using FE analysis.

Evolution of the calculated cutting forces with an increasing cutting length for different θ values of the (1 0 1) β-brass is shown in Fig. 4. Because of excessive distortion of elements in simulations for $\theta = -20°$ and $\theta = 20°$, the analysis did not complete; hence, the corresponding results for the cutting force were not included in Fig. 4. The cutting force was found to vary with different cutting directions. For instance, the measured value of the cutting force at the [1.414 −2 −1.414], [0.990 −2 −0.990], [−0.990 −2 0.990] and [−1.414 −2 1.414] directions corresponding to $\theta = -45°$, $-35°$, 35° and 45°, respectively, are larger compared to that in the [0 −1 0] directions ($\theta = 0°$). It should be emphasized that the fluctuations in the calculated cutting force occurred due to: (1) a small stable time increment used in analysis, where dynamic response associated with stress waves moving through the material (and reflecting at boundaries) were captured in the overall cutting force response; (2) reorientation of the local mesh during cutting process leading to a variation in the shear angle [10, 27]. These perturbations in the reaction force may be eliminated by introducing additional damping in the model, which would decrease the stable time increment thus making the analysis computationally expensive.

FE simulations were also performed using the EMCP theory. The results obtained with this approach demonstrate that while the EMSGCP theory predicted a cutting force that increased with an increase in the cutting length, the EMCP theory predicted the force value, stabilised at larger cutting-length magnitudes (Fig. 4). These observations are valid for all the studied cutting directions. The difference in the predicted cutting forces for the two theories was due to the fact that the EMSGCP theory characterises the contribution of strain gradients and its evolution during the inhomogeneous cutting process, and, hence, the strain-hardening rate was higher. The averages of force magnitudes for the cutting lengths of 1.0 μm and 1.75 μm were calculated; they are listed in Table 3 (F_{EMCP} and F_{EMSGCP} are the cutting force obtained with the EMCP and EMSGCP theories, respectively). As expected, the values predicted with the EMSGCP theory were noticeably larger when compared to those based on the EMCP theory. It was noted that the extent of respective difference was more significant for $\theta = 0°$ and $\theta = 35°$ than that for $\theta = -35°$ and $\theta = 45°$.

The levels of specific cutting energy were calculated based on the obtained cutting forces for different *d.o.c.* (0.8–2.0 μm) to investigate the size effect in micromachining of a f.c.c. single crystal. The EMSGCP theory was found to be more in accord with the experiments compared to the EMCP theory.

Apparently, the observed differences in realisation of micro-cutting in different directions should be underpinned by some processes at micro scale. Figure 5 presents the distributions of the sum of magnitudes of effective GND density in all the slip

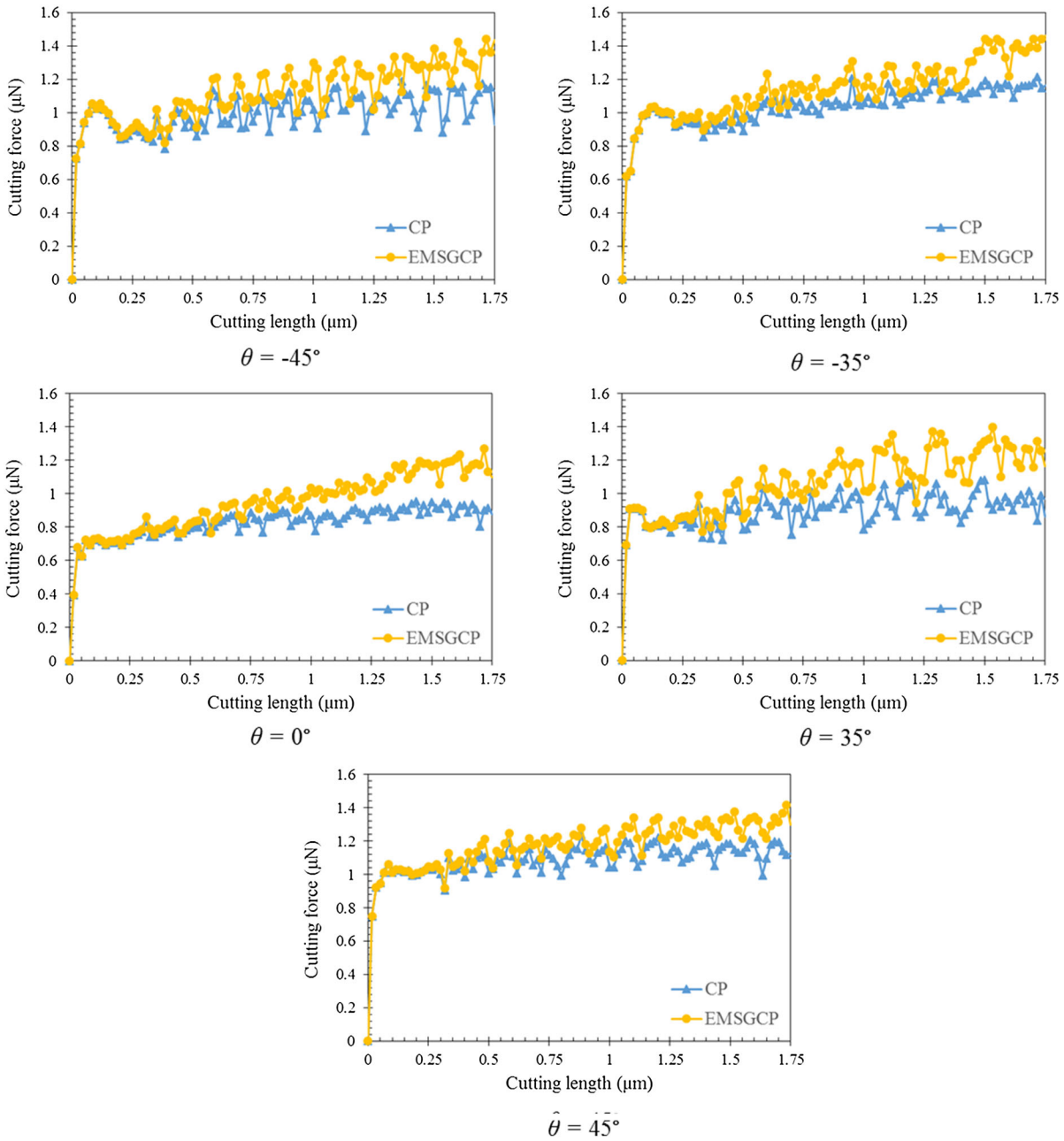

Fig. 4 Evolution of cutting forces obtained using EMSGCP and EMCP theories for different cutting directions

systems $\left(\sum_\alpha \left|n_G^{(\alpha)}\right|\right)$ for different cutting directions. This indicates that the effect of GNDs is significant on the chip surface in contact with the tool for $\theta = 0°$ and $\theta = 45°$, whereas for other orientations, it is higher both on the surface and in the primary deformation zone (PDZ), but with a larger magnitude in the former. It was observed that both the magnitude of the GND effect and its extent for $\theta = 45°$ were less compared to other orientations. This explains the correspondingly smaller relative difference of ~ 10 % in F_{EMCP} and F_{EMSGCP} for this orientation (Table 3) with respect to others. To get an insight into the distribution of GNDs, the total accumulative shear strain on all slip systems,

Table 3 Average cutting forces obtained with EMSGCP and EMCP theories and their relative differences for different θ values

θ	F_{EMCP} (μN)	F_{EMSGCP} (μN)	$(F_{EMSGCP} - F_{EMCP})/F_{EMSGCP}$ (%)	Chip compression ratio
−45°	1.064	1.251	17.53	0.82
−35°	1.127	1.276	13.21	0.86
0°	0.891	1.104	23.91	1.16
35°	0.945	1.207	27.65	0.84
45°	1.148	1.265	10.19	1.17

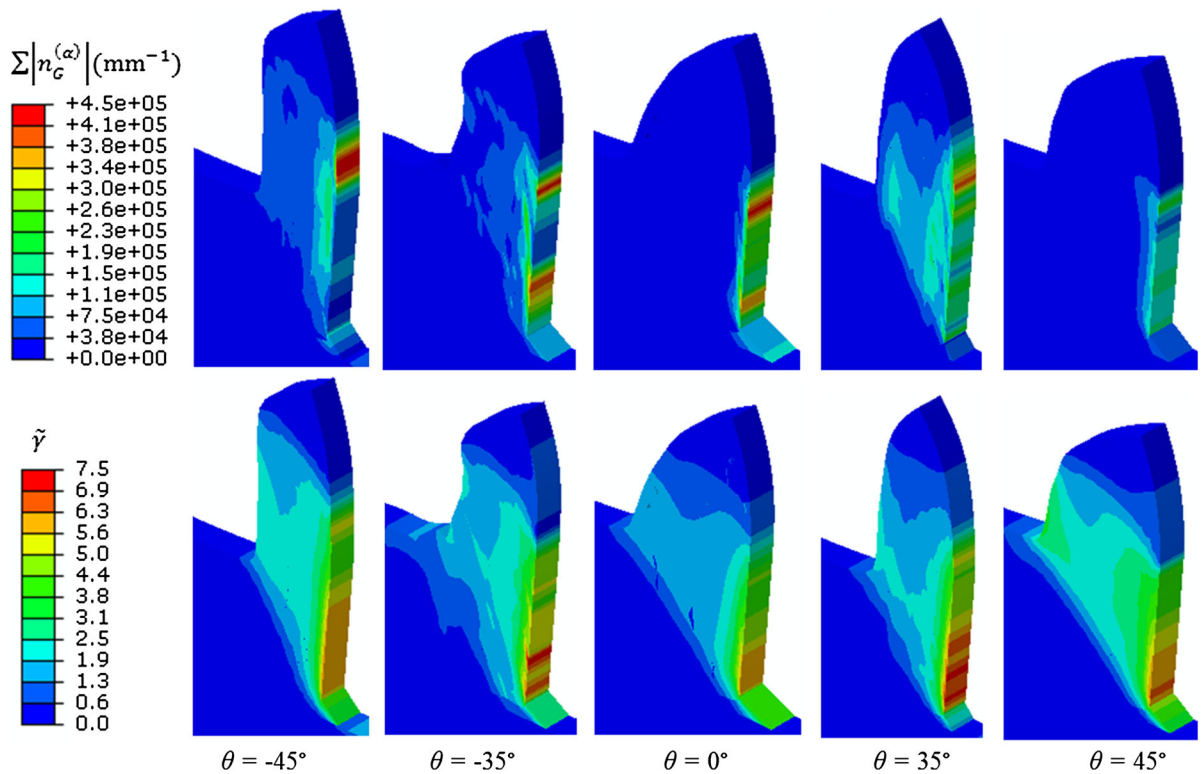

Fig. 5 Distribution of effective density of GNDs in all slip systems $\sum_\alpha \left|n_G^{(\alpha)}\right|$ (*top*) and total accumulative shear strain on all slip systems ($\tilde{\gamma}$) (*bottom*) at cutting length of 1.2 μm obtained with FE simulations using EMSGCP theory for (1 0 1) single-crystal β-brass for various θ

$\tilde{\gamma}$, was considered since their density is directly proportional to the gradients of effective plastic strain. For all the orientations, the shear activity was observed on both the chip surface and in the PDZ, but with a higher magnitude in the former. Interestingly, although its variation was observed in both regions for all the orientations, no GNDs evolved in the primary deformation zone for $\theta = 0°$ and $\theta = 45°$. This can be explained by the level of chip thickness after machining. Hence, a chip compression ratio (ratio of post-turning chip thickness to undeformed chip thickness) was calculated for all the cases investigated (Table 4). This ratio was higher for $\theta = 0°$ and $\theta = 45°$ due to larger post-turning thickness value. Since the GND density is proportional to the change in the effective plastic strain related to the size of the concerned region, for $\theta = 0°$ and $\theta = 45°$ the effect of GNDs was not significant in the PDZ due

Table 4 Parameters of calculated chip morphologies at cutting length of 1.2 μm for different crystal orientations and Taylor coefficients

θ	Taylor coefficient (α_T)	Shear angle	Post-turning chip thickness (μm)	Uncut chip thickness (nm)	Chip compression ratio
−45°	0.8		0.659	0.8	0.82
−35°	0.8		0.688	0.8	0.86
0°	0.8		0.927	0.8	1.16
35°	0.8		0.668	0.8	0.84
45°	0.0	45°	0.873	0.8	1.09
45°	0.8	42°	0.924	0.8	1.19
45°	1.6	39°	1.018	0.8	1.27

to larger post-turning chip thickness. Here, it should be emphasized that the EMSGCP being a lower-order theory does not require additional boundary conditions, preserving the classical structure of conventional plasticity theories, in contrast to proposed higher-order theories.

The influence of strain gradient on chip morphology was also investigated. Figure 6a presents the chip shapes obtained with the EMCP and EMSGCP theories (with different Taylor coefficient α_T) for $\theta = 45°$. It is worth mentioning that higher α_T values imply larger strain gradients. A larger shear angle with a smaller post-turning chip thickness was obtained when the EMCP theory was used (Table 4). This can be explained as follows: in the absence of evolving strain gradients, the material's cumulative strength is predicted to be lower; hence, the chip is formed easier, and shear planes with larger angles are generated, resulting in smaller chip thickness. On the other hand, when strain gradients become prominent, higher cutting energy is required due to increased material's strength to generate the chip; hence, shear planes with smaller angles are obtained, resulting in larger post-turning chip thickness.

During the micro-cutting processes, as the material progressively deforms, the lattice rotates considerably. Figure 6a demonstrates reorientation of the crystalline lattice about the axis parallel to the observation direction for different α_T values. A significant texture evolution, up to 45°, in the PDZ was observed for all the cases. Apparently, lattice rotations in the PDZ were overestimated by the EMCP theory. This can be explained as follows: as the mismatch in the lattice spin due to imposed boundary conditions for a material point can be accommodated by GNDs, the orientation change predicted by the EMSGCP is less distinct in comparison to that for the EMCP theory [28].

Niordson and Hutchinson [29] studied physical acceptability of a lower-order strain-gradient theory and observed a vertex in the plastic strain distribution when a finite layer was subjected to shear, which is an unexpected non-physical result. When the total accumulated shear strain on all slip systems, $\tilde{\gamma}$, on path A–B (shown in Fig. 6a) is plotted for the investigated cases (Fig. 6b), the distributions of plastic shear strain are smoother (with an increase in α_T) indicating that the predictions from EMSGCP are in line with expectations from a physically reasonable strain-gradient theory.

4 Concluding remarks

In this paper, a numerical implementation of an enhanced model of strain-gradient crystal plasticity was used to demonstrate predictive capabilities of the theory in assessment of the effect of evolved strain gradients on the cutting process for different cutting directions of b.c.c. single crystals of β-brass. The shear angles predicted for different θ values using our FE model are in better agreement with the experimental data than those obtained analytically. It was noted that the spatial positions of evolved GNDs varied considerably: for one orientation, they were mostly localised on the chip surface while in other cases they also evolved in the primary shear zone. Both chip morphology and texture evolution during the cutting process were affected significantly when the evolution of GNDs was accounted for in the constitutive equations. In this study, only mechanical processes—most prominent in micro-cutting—were considered.

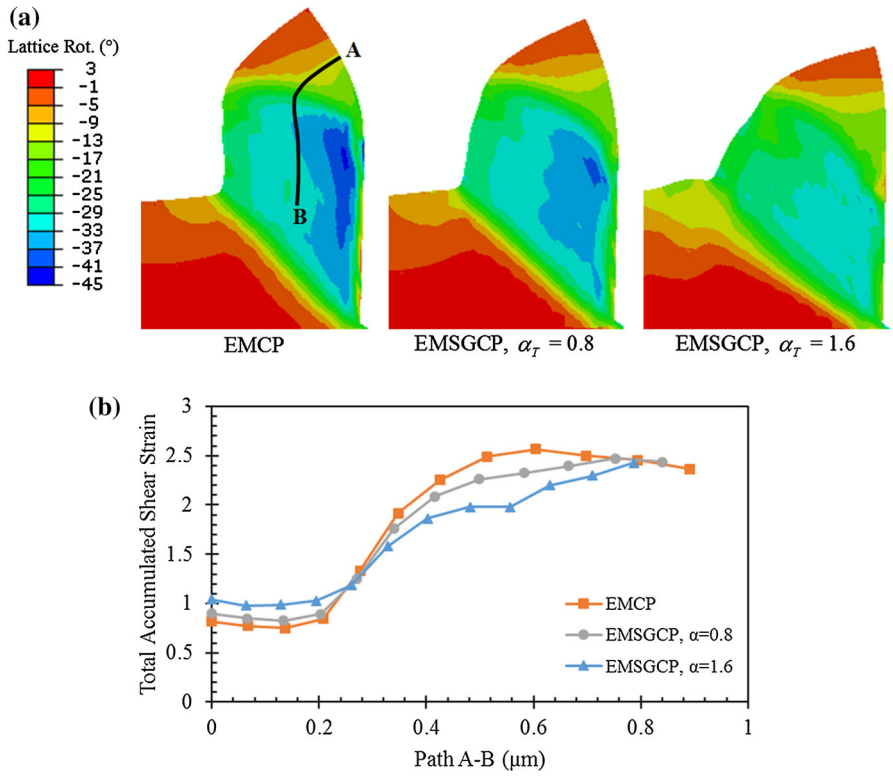

Fig. 6 **a** Distribution of lattice rotations on deformed configurations at cutting length of 1.2 μm obtained with FE simulations using EMCP and EMSGCP theories for $\theta = 45°$. **b** Total accumulated shear strain on all slip systems along path *A–B* (**b**) at cutting length of 1.2 μm

The next natural step would be to further develop the suggested approach incorporating frictional and thermal effects. There is much debate as to the nature of frictional laws especially with regard to small scale cutting. These matters aside, the presented model and corresponding results are not expected to change qualitatively.

Acknowledgments M.D. was supported with a fellowship from The Scientific and Technological Research Council of Turkey (TÜBITAK 2232, Project No: 114C199). A.R. and V.S. acknowledge funding from the Engineering and Physical Sciences Research Council (UK) through Grant EP/K028316/1 and Department of Science and Technology (India), project MAST.

Appendix

An enhanced modelling scheme for a strain-gradient crystal-plasticity (EMSGCP) theory proposed by Demiral [14] was used in the simulations. In the EMSGCP theory, the *critical resolved shear stress* (CRSS) ($g_T^\alpha|_{t=0}$) is governed by the initial strength of slip systems related to SSDs ($g_S^\alpha|_{t=0}$) and GNDs ($g_G^\alpha|_{t=0}$), linked with initial SSD ($\rho_S|_{t=0}$) and GND ($\rho_G|_{t=0}$) densities via the constant, K:

$$g_T^\alpha|_{\mathrm{t=0}} = \sqrt{\left(g_S^\alpha|_{\mathrm{t=0}}\right)^2 + \left(g_G^\alpha|_{\mathrm{t=0}}\right)^2}, \tag{1a}$$

$$\begin{aligned} g_S^\alpha|_{\mathrm{t=0}} &= K\sqrt{\rho_S|_{\mathrm{t=0}}}, \\ g_G^\alpha|_{\mathrm{t=0}} &= K\sqrt{\rho_G|_{\mathrm{t=0}}} = K\sqrt{\rho|_{\mathrm{t=0}}(\bar{S}/\bar{V})^2}. \end{aligned} \tag{1b}$$

The GND density term was expressed as a function of the normalized surface-to-volume ($\bar{S}/\bar{V}$) ratio (hence, dimensionless) for the component under study [30]. The slip resistance during loading evolves with hardening due to the SSDs (Δg_S^α) and GNDs (Δg_G^α) on the slip system as follows:

$$g_T^\alpha = g_T^\alpha|_{t=0} + \sqrt{\left(\Delta g_S^\alpha\right)^2 + \left(\Delta g_G^\alpha\right)^2}, \tag{1c}$$

$$\Delta g_S^\alpha = \sum_{\beta=1}^{N} h_{\alpha\beta}\Delta\gamma^\beta,\ \Delta g_G^\alpha = \alpha\mu\sqrt{b n_G^\alpha}, \tag{1d}$$

where $h_{\alpha\beta}$, α_T, μ, b and n_G^α corresponds to the slip-hardening modulus, the Taylor coefficient, the shear

modulus, the Burgers vector and the effective density of geometrically necessary dislocations, respectively.

The hardening model proposed by Peirce et al. [24] was used to describe $h_{\alpha\beta}$, as follows:

$$\begin{aligned} \mathrm{h}_{\alpha\alpha} &= \mathrm{h}_0 \mathrm{sech}^2 \left| \frac{\mathrm{h}_0 \tilde{\gamma}}{g_T^{\alpha}|_{\mathrm{sat}} - g_T^{\alpha}|_{\mathrm{t}=0}} \right|, \\ \mathrm{h}_{\alpha\beta} &= q \mathrm{h}_{\alpha\alpha} (\alpha \neq \beta), \\ \tilde{\gamma} &= \sum_{\alpha} \int_0^t |\dot{\gamma}^{\alpha}| dt, \end{aligned} \tag{2}$$

where h_0 is the initial hardening parameter, $g_T^{\alpha}|_{\mathrm{sat}}$ is the saturation stress of the slip system α, q is the latent hardening ratio, and $\tilde{\gamma}$ is the Taylor cumulative shear strain on all slip systems. The effective GND density (n_G^{α}) is given by

$$\mathrm{n}_G^{\alpha} = \left| \boldsymbol{m}^{\alpha} \times \sum_{\beta} s^{\alpha\beta} \nabla \gamma^{\beta} \times \boldsymbol{m}^{\beta} \right|, \tag{3}$$

where $\boldsymbol{s}^{\alpha}$ is the slip direction, $\boldsymbol{m}^{\alpha}$ is the slip-plane normal, $s^{\alpha\beta} = \boldsymbol{s}^{\alpha}.\boldsymbol{s}^{\beta}$ and $\nabla \gamma^{\beta}$ is the gradient of shear strain in each slip system [24].

In Eq. (2), $\dot{\gamma}^{\alpha}$ is the shearing rate on the slip system α expressed by the following power-law equation:

$$\dot{\gamma}^{\alpha} = \dot{\gamma}_0^{\alpha} \mathrm{sgn}(\tau^{\alpha}) \left| \frac{\tau^{\alpha}}{g_T^{\alpha}} \right|^n, \tag{4}$$

where $\dot{\gamma}_0^{\alpha}$, n, τ^{α} and g_T^{α} are the reference strain rate, the macroscopic rate-sensitivity parameter, the resolved shear stress, the strength of the slip system α at the current time, respectively, and $\mathrm{sgn}(*)$ is the signum function of *. In an enhanced model of crystal-plasticity (EMCP) Δg_G^{α} is assumed to be equal to 0.

References

1. Lawson BL, Kota N, Ozdoganlar OB (2008) Effects of crystallographic anistropy on orthogonal micromachining of single-crystal aluminum. J Manuf Sci Eng 130(3):031116
2. Sato M, Kato K, Tuchiya K (1978) Effect of material and anisotropy upon the cutting mechanism. Trans Jpn Inst Met 9:530–536
3. Sato M, Kato Y, Aoki S, Ikoma A (1983) Effects of crystal orientation on the cutting mechanism of the aluminum single crystal: 2nd report: on the (111) plane and the (112) end cutting. Bull JSME 26(215):890–896
4. Shirakashi T, Yoshino M, Kurashima H (1991) Study on cutting mechanism of single crystal based on simple shear plane model. Int J Jpn Soc Precis Eng 25(2):96–97
5. Lee WB, Zhou M (1993) A theoretical analysis of the effect of crystallographic orientation on chip formation in micro-machining. Int J Mach Tools Manuf 33:439–447
6. Lee WB, Cheung CF, To S (2002) A microplasticity analysis of micro-cutting force variation in ultra-precision diamond turning. J Manuf Sci Eng 124(2):170–177
7. Kota N, Ozdoganlar OB (2010) A model-based analysis of orthogonal cutting for single-crystal fcc metals including crystallographic anisotropy. Mach Sci Technol 14(1):102–127
8. Liang Y, Moronuki N, Furukawa Y (1994) Calculations of the effect of material anisotropy on microcutting processes. Precis Eng 16(2):132–138
9. Liu K, Melkote SN (2007) Finite element analysis of the influence of tool edge radius on size effect in orthogonal micro-cutting process. Int J Mech Sci 49:650–660
10. Zahedi SA, Demiral M, Roy A, Silberschmidt VV (2013) FE/SPH modelling of orthogonal micro-machining of f.c.c. single crystal. Comput Mater Sci 78:104–109
11. Demiral M, Roy A, El Sayed T, Silberschmidt VV (2014) Numerical modelling of micro-machining of fcc single crystal: influence of strain gradients. Comput Mater Sci 94:273–278
12. Huang Y, Qu S, Hwang KC, Li M, Gao H (2004) A conventional theory of mechanism-based strain gradient plasticity. Int J Plast 20(4):753–782
13. Ertürk I, Van Dommelen JAW, Geers MGD (2014) Gradient crystal plasticity modelling of anelastic effects in particle strengthened metallic thin films. Meccanica 49:2657–2685
14. Demiral M (2012) Enhanced gradient crystal-plasticity study of size effects in b.c.c. metal. Dissertation, Loughborough University, UK
15. Arsenlis A, Parks DM, Becker R, Bulatov VV (2004) On the evolution of crystallographic dislocation density in non-homogeneously deforming crystals. J Mech Phys Solids 52(6):1213–1246
16. Bardella L (2006) A deformation theory of strain gradient crystal plasticity that accounts for geometrically necessary dislocations. J Mech Phys Solids 54(1):128–160
17. Kuroda M, Tvergaard V (2008) On the formulations of higher-order strain gradient crystal plasticity models. J Mech Phys Solids 56(4):1591–1608
18. Gurtin ME (2008) A finite-deformation, gradient theory of single-crystal plasticity with free energy dependent on densities of geometrically necessary dislocations. Int J Plast 24(4):702–725
19. Dassault Systemes (2013) Abaqus 6. 13 analysis user manual
20. Ueda K, Iwata K, Nakayama K (1980) Chip formation mechanism in single crystal cutting of β-brass. CIRP Ann Manuf Tech 29(1):41–46
21. Jona F, Marcus PM (2001) Structural and elastic properties of β-brass. J Phys: Condens Matter 13(23):5507
22. Jia N, Roters F, Eisenlohr P, Kords C, Raabe D (2012) Non-crystallographic shear banding in crystal plasticity FEM simulations: example of texture evolution in α-brass. Acta Mater 60(3):1099–1115

23. Beyerlein IJ, Mara NA, Bhattacharyya D, Alexander DJ, Necker CT (2011) Texture evolution via combined slip and deformation twinning in rolled silver–copper cast eutectic nanocomposite. Int J Plast 27(1):121–146
24. Peirce D, Asaro R, Needleman A (1982) An analysis of nonuniform and localized deformation in ductile single crystals. Acta Metall 30:1087–1119
25. Schulze D, Paufler P (1979) Physikalische Grundlagen-mechanischer Festkörpereigenschaften. Akademie-Verlag, Berlin
26. Lee WB (1990) Prediction of microcutting force variation in ultra-precision machining. Precis Eng 12(1):25–28
27. Tajalli SA, Movahhedy MR, Akbari J (2014) Simulation of orthogonal micro-cutting of FCC materials based on rate-dependent crystal plasticity finite element model. Comput Mater Sci 86:79–87
28. Demiral M, Roy A, El Sayed T, Silberschmidt VV (2014) Influence of strain gradients on lattice rotation in nano-indentation experiments: a numerical study. Mater Sci Eng, A 94:273–278
29. Niordson CF, Hutchinson JW (2003) On lower order strain gradient plasticity theories. Eur J Mech A Solids 22(6):771–778
30. Demiral M, Roy A, Silberschmidt VV (2013) Indentation studies in bcc crystals with enhanced model of strain-gradient crystal plasticity. Comput Mater Sci 79:896–902